Solar Physics
DOI: 10.1007/•••••-•••-•••-••••-•

Coronal Shock Waves, EUV waves, and their Relation to CMEs. I. Reconciliation of "EIT waves", Type II Radio Bursts, and Leading edges of CMEs

V.V. Grechnev[1] · **A.M. Uralov**[1] · **I.M. Chertok**[2] · **I.V. Kuzmenko**[3] · **An.N. Afanasyev**[1] · **N.S. Meshalkina**[1] · **S.S. Kalashnikov**[1] · **Y. Kubo**[4]

© Springer ••••

Abstract We show examples of excitation of coronal waves by flare-related abrupt eruptions of magnetic rope structures. The waves presumably rapidly steepened into shocks and freely propagated afterwards like decelerating blast waves that showed up as Moreton waves and EUV waves. We propose a simple quantitative description for such shock waves to reconcile their observed propagation with drift rates of metric type II bursts and kinematics of leading edges of coronal mass ejections (CMEs). Taking account of different plasma density falloffs for propagation of a wave up and along the solar surface, we demonstrate a close correspondence between drift rates of type II bursts and speeds of EUV waves, Moreton waves, and CMEs observed in a few known events.

Keywords: Coronal Mass Ejections, Low Coronal Signatures; Coronal Mass Ejections, Initiation and Propagation; Prominences, Active; Radio Bursts, Dynamic Spectrum; Radio Bursts, Type II; Waves, Shock

1. Introduction

Some solar eruptions are accompanied by large-scale wave-like disturbances visible in various spectral ranges. Moreton waves observed in the chromospheric Hα line have been known for a long time (Moreton, 1960). Uchida (1968) proposed a theoretical model, which considered a Moreton wave as a chromospheric trail

[1]Institute of Solar-Terrestrial Physics SB RAS, Lermontov St. 126A, Irkutsk 664033, Russia email: grechnev@iszf.irk.ru
[2] Pushkov Institute of Terrestrial Magnetism, Ionosphere and Radio Wave Propagation (IZMIRAN), Troitsk, Moscow Region, 142190 Russia email: ichertok@izmiran.ru
[3] Ussuriysk Astrophysical Observatory, Solnechnaya St. 21, Primorsky Krai, Gornotaezhnoe 692533, Russia email: kuzmenko_irina@mail.ru
[4] National Institute of Information and Communications Technology, Tokyo, Japan email: kubo@nict.go.jp

of a coronal fast-mode MHD wave. Observations of the low corona in extreme ultraviolet (EUV) emission lines with EIT (Delaboudinière *et al.*, 1995) on SOHO revealed large-scale wave-like disturbances visible as fronts of enhanced (but still low) brightness, either quasi-stationary or propagating over large distances up to the whole disk along the solar surface or expanding above the limb. These transients called "EIT waves" (or "EUV waves") are registered by a number of EUV telescopes — EIT, TRACE, STEREO/EUVI, SDO/AIA, *etc.* (see Wills-Davey and Attrill, 2009; Gallagher and Long, 2010 for a review).

Analysis of observations and interpretation of such phenomena meet problems. Glaring flare emission hampers detection of faint EUV waves. Many data are limited by 12-min imaging rate of EIT. Faster TRACE observations (Handy *et al.*, 1999) have a small field of view. It is often difficult to reliably identify and trace a moving feature of interest [this is also related to eruptions and coronal mass ejections (CMEs)]. Multi-instrument analyses sometimes encounter timing problems. To overcome these difficulties, special methods are employed, but they might contribute artifacts. Thus, some results used in interpretation and modeling might not be completely adequate to the observed phenomena.

The nature of EUV waves has been debated starting from their discovery (Thompson *et al.*, 1998). The most popular interpretations of a near-surface EUV wave are *i*) a manifestation of an MHD fast-mode wave in the lower corona (*e.g.*, Thompson *et al.*, 1999; Warmuth *et al.* 2001, 2004b; Khan and Aurass, 2002; Hudson and Warmuth, 2004) and *ii*) a transient plasma compression in bases of coronal loops in their successive stretching by an expanding CME (*e.g.*, Delannée and Aulanier, 1999). A numerical 2D MHD simulation of a magnetic flux rope eruption (Chen, Fang, and Shibata, 2005) revealed both the (*i*) and (*ii*) disturbances. Schmidt and Ofman (2010) presented the first 3D MHD modeling of an "EIT wave" as a disturbance produced by the rear of a shock wave driven by an eruption. A fast-mode wave detected in this numerical experiment corresponded to an EUV wave actually observed in the modeled event including reflection from a coronal hole in support of the wave hypothesis.

None of existing models describes the whole set of observational facts related to EUV waves. Most likely, this is not only due to limitations of theoretical models or observational issues listed above, but also because the multitude of transients observed as EUV waves actually correspond to different phenomena. This conjecture is supported by a variety of morphologic and dynamic characteristics of observed EUV waves. For example, 1) their velocities estimated from observations of some events exceeded the coronal fast-mode speed, whereas they were lower in other events; 2) the wave front can be either diffuse or sharp; 3) their kinematics can be incompatible with the fast-mode MHD wave model (Zhukov, Rodriguez, and de Patoul, 2009). On the other hand, such properties of EUV waves as deceleration, decay, and broadening the disturbance (Warmuth *et al.* 2001, 2004a, 2004b; Long *et al.*, 2008; Veronig *et al.*, 2010), bypassing regions of an increased Alfvén velocity — coronal holes and active regions (Thompson *et al.*, 1999), possible reflections (Veronig, Temmer, and Vršnak, 2008; Gopalswamy *et al.*, 2009) appear to correspond to the hypothesis of a coronal MHD wave.

Considerations of wave-like transients sometimes observed in EUV to expand above the limb also suggest that different phenomena might be involved (*e.g.*,

Zhukov and Auchère, 2004). For example, an off-limb "EIT wave" presented by Chertok, Grechnev, and Uralov (2009) was most likely an expanding structural component of CMEs launched by a filament eruption outside of active regions (similar examples were shown by Grechnev *et al.*, 2006c), while an on-disk "EIT wave" in the same event appeared to be the case, which Delannée and Aulanier (1999) and Chen, Fang, and Shibata (2005) were talking about. Studies of an impulsive eruptive flare event by Grechnev *et al.* (2008) and Pohjolainen, Hori, and Sakurai (2008) led all the authors to a conclusion that an "EIT wave" observed both on the disk and off-limb was a manifestation of a coronal shock wave. Meshalkina *et al.* (2009) revealed in an impulsive event rapidly propagating manifestations of a shock wave both on the disk and above the limb, while another brightening slowly moving within a limited region resembled the situation modeled by Chen, Fang, and Shibata (2005).

If some EUV waves are due to coronal shock waves, then correspondence with signatures of shocks in the higher corona is expected. Type II radio bursts are considered as manifestations of shock waves propagating upwards in the corona (*e.g.*, Vršnak and Cliver, 2008). However, Klassen *et al.* (2000) concluded that almost all metric type II bursts were accompanied by EUV waves but stated no correlation between their speeds; the EUV waves speeds on average were three times less than estimates from drift rates of type II bursts. Biesecker *et al.* (2002) found that many EUV waves were not associated with type II bursts.

Sheeley, Hakala, and Wang (2000) concluded that kinks or deflections of coronal rays pronounced at the flanks and rear ends of fast CMEs visible in SOHO/LASCO images could be signatures of shock waves. An important common property established for these flank/rear kinks was their deceleration, while the authors did not reveal deceleration of CME leading edges[1]. However, a usually considered scenario for the formation of shock waves, which might show up in LASCO images, seems to be incompatible with wave signatures on the solar surface. In this scenario, when the velocity of a CME exceeds the local fast-mode speed at heliocentric distances $\gtrsim 1.5R_{\odot}$, a bow shock forms continuously pressed by a fast CME. However, a bow shock followed by a Mach cone can only be formed by a supersonic body of a fixed size, whereas CMEs expand omnidirectionally (with respect to their center). Hence, the conic bow shock geometry appears to be unlikely for wide CMEs. Since neither mechanisms nor heights of the shock formation have been established, possible association between surface EUV waves and CME components cannot be excluded. Indeed, Veronig *et al.* (2010) found the upper part of an expanding EUV dome to coincide with a white-light CME, while the lower skirt of the dome was a surface EUV wave.

For these reasons it is difficult to expect that all observed properties of EUV waves could be explained by a single mechanism. Based on this assumption, our three companion papers are focused on those EUV waves, which are most likely associated with coronal shock waves. We address a few events, all of which

[1]The SOHO LASCO CME Catalog at http://cdaw.gsfc.nasa.gov/CME_list/ (afterwards 'the CME Catalog'; Yashiro *et al.*, 2004) shows pronounced decelerations for three of the four events considered by the authors.

were previously studied. Even for a rather uniform subset of phenomena probably corresponding to similar processes, seemingly contradictions between some observational facts might occur. We endeavor to reconcile such discrepancies.

One of challenging issues listed above is reconciliation of EUV wave velocities and drift rates of type II bursts. This is a subject of the present paper I, the first one of three companion papers. Assuming the shock wave nature of EUV waves under consideration, we endeavor to settle disagreement between different studies and explain features revealed in analyzed events. In this paper we operate with a simplest approximation of a self-similar shock wave that is convenient in comparisons with observations, which often show self-similarity of the wave front expansion. However, this approximation corresponds to the strong shock wave limit and cannot apply to all stages of events. Considerations of a weaker shock seem to be more realistic. The case of a weak shock is more complex to calculate; paper II (Afanasyev and Uralov, 2010) is devoted to an analytic modeling of propagation of a weak shock along the solar surface. In paper III (Grechnev *et al.*, 2010) we address propagation of a probable shock wave in the 17 January 2010 event using both strong and weak shock approximations.

2. Methodical Issues

Excitation of coronal shock waves in eruptive flare events seems to be undoubted, but their sources have not yet been established. Three possible exciters of shock waves are considered: *i*) a pressure pulse produced by a flare, *ii*) a supersonic (superalfvénic) piston, *i.e.*, a CME, and *iii*) an impulsive piston. In case (*ii*) a bow shock continuously driven by a supersonic piston is expected to appear, whose kinematics is determined by the driver. In cases (*i*) or (*iii*) the shock wave initially expelled by an impulsive driver propagates afterwards freely like a decelerating blast wave (*cf.* Pomoell, Vainio, and Kissmann, 2008).

Observations suggest that shock waves excited by impulsive drivers and freely propagating in the low corona do exist as indicated by deceleration of Moreton/EUV waves (*e.g.*, Warmuth *et al.* 2001, 2004a), differences between propagation directions of the wave and a possible driver (Hudson *et al.*, 2003), very early appearance of type II bursts. We accept this possibility as a working hypothesis and use a description of the propagation of a blast shock wave. It is possible to calculate it analytically for two limits. One limit is a strong self-similar wave, whose length along the propagation direction is comparable with the curvature radius of the wave front. The opposite limit is a weak shock wave, whose length is much less than both the curvature radius of the front and typical sizes of inhomogeneities in the medium. Grechnev *et al.* (2008) found that a formal usage of expressions for propagation of a strong self-similar shock wave excited by a point-like explosion in a gas allowed to fit the speeds and positions of the Moreton wave as well as EUV wave at the initial stage of their motion.

2.1. Self-Similar Shock Wave Approximation

Grechnev *et al.* (2008) used a simple model to describe propagation of such a blast-like wave in plasma with a radial power-law (PL) density falloff δ from an

eruption center, $n = n_0(x/h_0)^{-\delta}$ with x being the distance and n_0 the density at a distance of h_0. We use $h_0 \approx 100$ Mm, close to the height scale. (*Our notations are different from those used in papers listed above*). Such a wave decelerates with $\delta < 3$ due to growing mass of swept-up material. Propagation of a strong shock vs. time t in plasma with a PL density model is described by an expression:

$$x(t) \propto t^{2/(5-\delta)} \tag{1}$$

The approximation has a singularity at $x \to 0$ (here also the wave velocity $v \to \infty$), but this is not crucial, because wave signatures are not observed at small distances. The approximation becomes inaccurate at large distances, being not limited from below by the fast-mode speed. A wave traveling along the solar surface weakens at large distances and propagates, in the first approximation, in a flat-layered atmosphere. Expression (1) was obtained for a strong spherical shock wave, which seems to be unrealistic in solar conditions, but its usage within some range of distances can be justified. 1) An enhanced plasma density above an active region falls off both vertically and horizontally. A power-law description of the falloff seems to be acceptable. 2) The self-similar solution of a strong wave is known to satisfactorily describe damping of a gas-dynamic shock wave up to Mach numbers $M \approx 2$, when the wave is neither strong nor weak. 3) Applicability of gas-dynamic self-similar solutions to MHD blast shock waves is not obvious, because account of the strength and geometry of the magnetic field appears to be necessary. We note in this respect the following. With $M \gg 2$, the gas pressure behind the shock front exceeds the magnetic pressure, even if $\beta = C_S^2/V_A^2 \ll 1$ in non-disturbed plasma before the shock front; here M is a ratio of the shock front speed to the fast-mode speed before the front, C_S and V_A are the sound and Alfvén speeds. That is, the plasma flow behind the shock front has a gas-dynamic character. The role of magnetic fields is also not crucial for medium-intensity shocks ($M \geq 2$), which also strongly heat plasma, significantly increasing its pressure. For example, with $M \approx 2$, the plasma pressure behind the front of a wave perpendicular to the magnetic field is equal to the magnetic pressure before the front, even if $\beta \ll 1$ there. For a switch-on shock wave running along the magnetic field this occurs with a Mach number $M \approx 1.5$.

Expression (1) was obtained under an assumption that the δ index was independent of the wave propagation direction. We will formally use this expression also when $\delta = \delta(\vartheta)$, if variations of δ are small with the change of the direction, *i.e.*, $\pi d\delta \ll d\vartheta$. Note that in the limit of a weak, short shock wave, its propagation is determined by a local value of δ even if this condition is not satisfied. The above considerations lead to a heuristic conclusion about a possibility to use expression (1) for approximate estimates of kinematic characteristics of shock waves of intermediate intensity propagating in medium with $\delta = \delta(\vartheta)$.

2.2. Coronal density models

It is useful to compare the power-law model with other popular density models. The Newkirk (1961) model ($n_e = 4.2 \times 10^4 \times 10^{4.32/r}$, r is the heliocentric

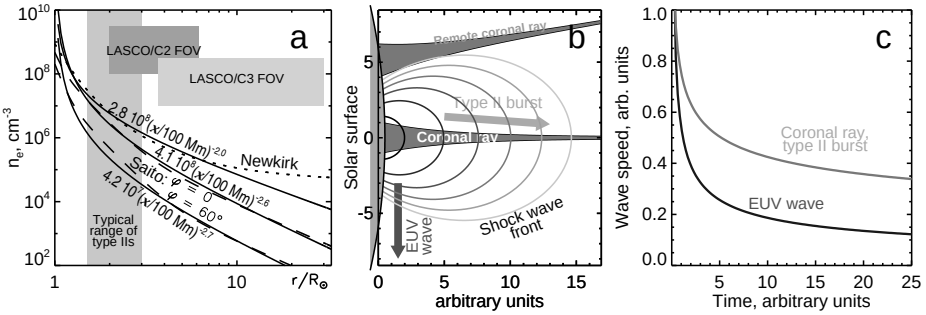

Figure 1. a) Coronal density models of Newkirk (dotted) and Saito (dashed, for latitudes $\varphi = 0°$ and $\varphi = 60°$). The solid lines represent the power-law model with different parameters to fit the Newkirk model at $r < 9R_\odot$ and the Saito model within the LASCO/C2 & C3 fields of view shown with shading. The vertical shaded region indicates the typical range of type II bursts. b) A cartoon illustrating the relation between a type II burst and an EUV wave. A narrowband type II emission is generated by a shock front propagating in a distinct extended narrow structure like a coronal ray. A near-surface EUV wave runs slower. (c) Temporal changes of speeds of the EUV wave and the type II emission site.

distance expressed in solar radii) describes the radial plasma density distribution in a coronal streamer. The Saito model (Saito, 1970) describes the density distribution above the quiet Sun depending on the latitude φ

$$\frac{n_e(r,\varphi)}{10^8} = \frac{3.09}{r^{16}}(1 - 0.5\sin\varphi) + \frac{1.58}{r^6}(1 - 0.95\sin\varphi) + \frac{0.0251}{r^{2.5}}(1 - \sin^{0.5}\varphi) \quad (2)$$

Figure 1a presents the Saito model for $\varphi = 0°, 60°$, and the Newkirk model. The PL model can be adjusted to any of these models by varying its parameters. The n_0, h_0 parameters are redundant; we have split them to clarify their physics meaning. The x variable of the PL model in the radial direction is $x \approx (r-1)R_\odot$. The PL model with $\delta = 2$, $n_0 = 2.8 \times 10^8$ cm^{-3} agrees within $\pm 30\%$ with the Newkirk model at $r = (1.2-9)R_\odot$ that is important for considerations of type II bursts. The parameters of the PL model can be adjusted to the Saito model for various φ as well, that is important for considerations of CMEs observed with LASCO/C2 & C3. A single PL model with a direction-dependent δ provides a convenient alternative to complex involvement of various density models (*cf.*, *e.g.*, Pohjolainen, Hori, and Sakurai, 2008). Advantages of the PL model are also determined by the account of individual properties of an active region as well as highly disturbed conditions just before the appearance of a wave.

2.3. Shock Waves and Type II Bursts

Assuming δ to depend on a propagation direction, we get an illustrative approximation for a shock, which is neither strong nor weak and propagates in an anisotropic medium as Figure 1b outlines. A quasi-isotropic shock wave propagating in the corona can only cause drifting continuum radio emission. A strong narrowband harmonic type II emission can appear if the shock front passes along a narrow extended structure like a coronal streamer (see, *e.g.*, Reiner *et al.*, 2003). The cumulation effect increases the density jump in vicinities

of the streamer's current sheet and intensifies radio emission (Uchida, 1974). The situation appears to resemble a flare-like process running along a coronal ray (Uralova and Uralov, 1994). Figure 1c outlines the difference between the horizontal and vertical directions to explain a relation between the speeds of an EUV wave and a type II burst. The wave center rises that determines a basically higher upwards speed than the surface one.

If the shock front encounters a remote coronal ray, then the intersection site might bifurcate with its parts moving along the ray in opposite directions (*cf.* Mancuso and Abbo, 2004). The contact corresponds to an infinite drift rate followed by bidirectional drifts visible as a (-like feature in a dynamic spectrum. Note that dynamic spectra present combination of emissions originating at different sites, so that the intensities are summed.

Based on these considerations, in the next Section we reconcile the kinematics of "EIT waves" measured from EUV images and drift rates of the corresponding type II bursts observed in dynamic spectra. We describe the kinematics of both wave signatures in terms of our heuristic approach based on the self-similar strong shock approximation outlined in Section 2.1. We apply power-law curves with the same onset to both spectral domains. The density falloff index in a streamer determining the drift rate of a type II burst is expected to be $\delta \sim 2$. Real lateral density falloffs in a streamer should be steeper ($\delta > 2$) than along its axis ($\delta \approx 2$). Otherwise, streamers would not be visible in homogeneous corona. Thus, real shock fronts should be oblate at medium distances. The lateral density falloff index for an EUV wave might be $0 < \delta < 3$. For possible wave signatures in CMEs, the density falloff index is expected to be close to the Saito model (2), i.e., $\delta \sim 2.6$ at moderate latitudes and steeper at higher latitudes.

In next sections we use an abbreviation "shock-PL" to denote considerations of shock waves traveling in the solar atmosphere in the approximation of a self-similar strong shock propagating in medium with a power-low density falloff.

3. Observations

3.1. Event 1: 13 July 2004

This event (Figure 2) was associated with an eruptive M6.7 flare (00:09–00:23, *all times hereafter are UT*) in active region 10646 (N13 W46) and a CME after 00:54 observed with SOHO/LASCO (Brueckner *et al.*, 1995). Two parts of the CME (Figure 2b,c) are listed in the CME Catalog as two CMEs measured at position angles of 294° and 213°. A type II burst was recorded in three observatories. The three estimates of the shock speed progressively decreased in time.

Grechnev *et al.* (2008) revealed manifestations of a probable blast wave as an Hα Moreton wave (gray in Figure 2a) and an EUV wave (white). Both disturbances were kinematically close to each other and to an expected trail of a decelerating coronal blast wave whose exciter was not discussed. The authors proposed that the decreasing estimations of the shock speed reflected deceleration of a single shock wave, but did not consider the type II burst.

Pohjolainen, Hori, and Sakurai (2008) [afterwards PHS] addressed other aspects of this event. They analyzed the type II burst but have not found a

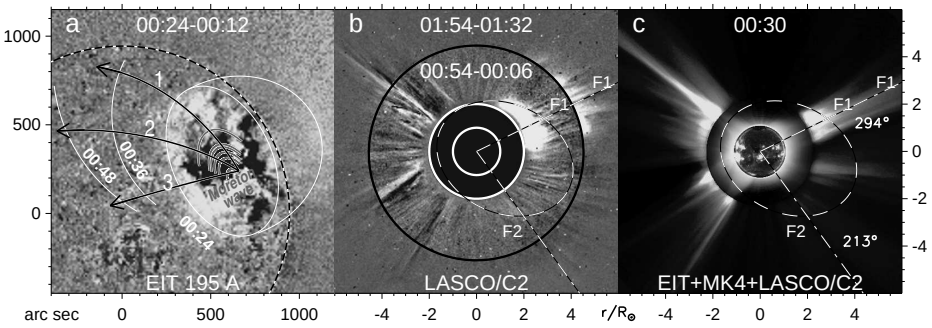

Figure 2. The 13 July 2004 event. a) The Moreton (gray) and EUV wave (white) fronts superposed on the EIT 195 Å difference image. The black arcs 1, 2, and 3 trace the directions of measurements. The dotted circle denotes the limb. (b) The leading part of the CME observed in two LASCO/C2 difference images at 00:54 and 01:54 separated with the black circle. c) The non-disturbed corona in a combined image composed from non-subtracted EIT 195 Å, Mark4, and C2 images. The dashed ovals in (b) and (c) outline the CME in the 00:54 image. The dash-dotted straight lines in (b) and (c) mark the position angles at which the measurements listed in the CME Catalog were carried out for the fastest features F1 and F2. Axes show distances from the solar disk center in arc seconds (a) and in solar radii (b and c).

reasonable way to reconcile the overall drift with propagation of a single shock wave. The authors proposed that two shock waves were excited, one by a flare blast and the second by an expanding loop, a part of an appearing CME.

We carried out an additional analysis of this event, measured the kinematics of an eruptive system in order to find out a probable origin of a shock wave(s), and to reconcile its (their) propagation with the EUV/Moreton waves.

3.1.1. Eruptive System

Figure 3 shows an eruptive system: a leading bright feature ('bf'), two dark filament segments and eruptive loops, one of which ('loop') was conspicuous. Long exposure times (33 – 46 s) caused blurring fast features, *e.g.*, a jetlike appearance of the bright feature (see Grechnev *et al.*, 2008).

To measure the expansion of a feature in question, we outline it with an oval arc that allows us to trace its expansion even if its leading edge is sometimes difficult to detect. In this way we get a distance-time plot and use it as an initial approximation. Then we choose a regular function to match the distance-time plot and estimate its parameters. Using the analytic fit, we calculate expected distance-time points, compare them with observations, and improve the fit. All kinematical plots are calculated by means of integration or differencing the analytic fit rather than experimental measurements. Our ultimate criterion is to approximately reproduce the motion of an analyzed feature.

Observational limitations do not allow us to reveal a detailed time profile of the acceleration. It seems to be reasonable instead to describe it with a smooth bell-like function. We use a Gaussian time profile (a similar fit was used by Wang, Zhang, and Shen, 2009). Then the acceleration a is

$$a = (v_1 - v_0)\exp\{-[(t - t_0)/\tau_{\rm acc}]^2/2\}/(\sqrt{2\pi}\tau_{\rm acc}) \qquad (3)$$

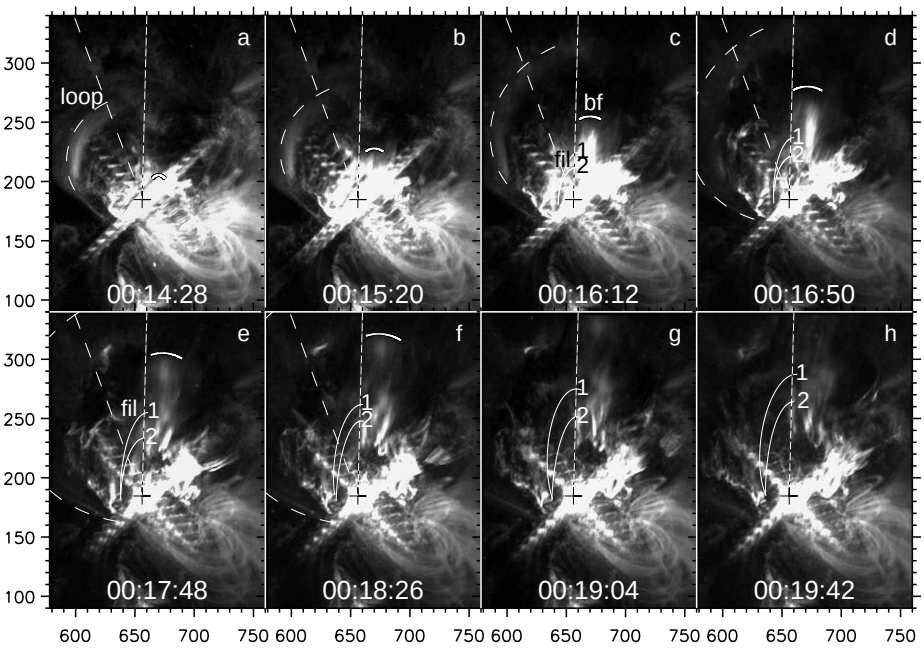

Figure 3. The eruptive system in the 13 July 2004 event observed with TRACE at 173 Å. The cross marks the initial position of a dark filament. Oval arcs outline the eruptive loop (dashed), dark filaments (solid), and the bright eruptive feature (short arc). The broken lines denote the expansion directions of the loop (dashed) and the filament top (dotted). Axes show arc seconds from the solar disk center.

Here $\tau_{\rm acc}\sqrt{8\ln 2}$ is a full width at half-maximum of the acceleration time profile, which is centered at the t_0 time, v_0 and v_1 are velocities at the onset and end of the acceleration stage. In cases when the kinematics is more complex, we use a combination of Gaussians and adjust their parameters manually.

The results of plane-of-sky measurements are shown in Figure 4 for the loop and bright feature (left) and for the filament segments (right). When the measurements began, the bright feature already rose that probably corresponded to the initiation phase, which started at about 00:07 according to GOES. A strong acceleration started at about 00:13, reached 4 km s^{-2}, and then changed to a significant deceleration. The loop was static by 00:14:30; after 00:15:10 its speed sharply changed to ≈ 320 km s^{-1} and did not increase afterwards. The transition from the initial zero speed to a final one occurred between two samples. Hence, the maximum acceleration of the loop could well exceeded 10 km s^{-2}.

Figure 4c also shows the plasma pressure computed from GOES soft X-ray (SXR) light curves with a source size of 15 Mm found from RHESSI images. The pressure gradually rose while the bright feature suddenly started to decelerate. Thus, the flare pressure was unlikely a driver of either the eruption or the wave, whose estimated start time is delimited with vertical dashed lines.

Measurements of the filament segments 1 and 2 are shown in Figure 4 along with average plots for the filament denoted with the solid lines. The filament started to rise nearly simultaneously with the bright feature. However, both the

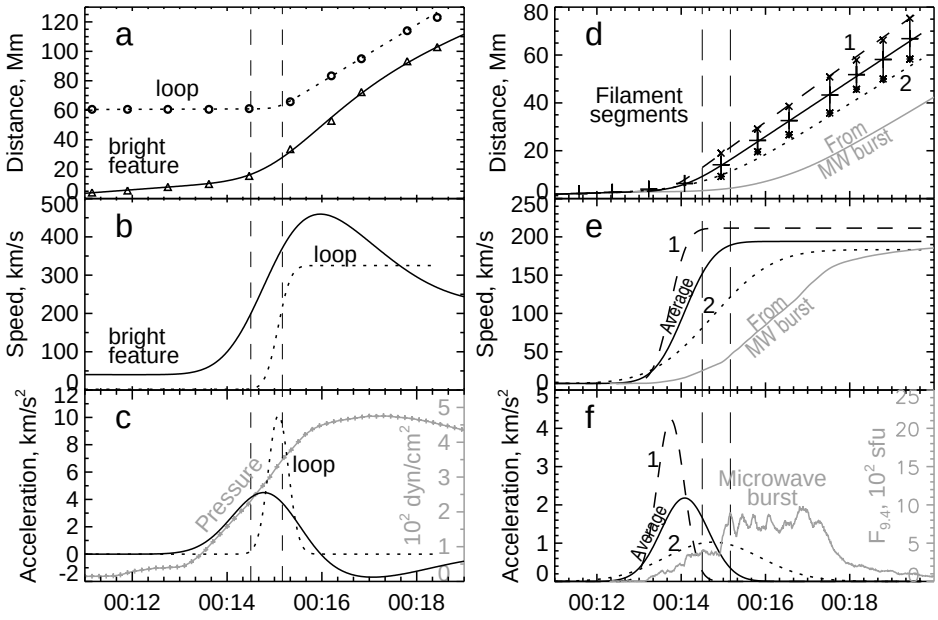

Figure 4. Kinematic plots of the eruptions in the 13 July 2004 event: the loop and bright feature (left) and the filament segments 1 and 2 (right; the solid curves correspond to averages between 1 and 2). Symbols mark the measured plane-of-sky distances, and curves represent their fit. The gray curve in panel (c) displays the plasma pressure computed from GOES SXR fluxes. The gray curves in panels (d – f) show kinematical plots calculated assuming the correspondence of the acceleration plot to the microwave one. The vertical dashed lines delimit the start time of the wave estimated by Grechnev *et al.* (2008).

acceleration and speed of the bright feature were higher; it obviously surpassed the filaments (see Figure 3). The nature of this feature is difficult to identify from observations. In some images it resembles an arcade surrounding the filament; however, initially it seems to be located below the filament. The bright feature might be also one more filament, which underwent heating and therefore brightened. An additional possibility is suggested by a scenario proposed by Meshalkina *et al.* (2009): this feature might be a small-scale magnetic rope whose eruption destabilized the filament. In any case, the measurements suggest that just the bright feature was the major driver of the eruption.

The gray curves in Figure 4d – f also show kinematical plots calculated under the assumption that the acceleration plot corresponded to the 9.4 GHz light curve. Microwave fluxes are known to be close in shape to hard X-ray (HXR) ones, while the acceleration of eruptions has been found to be close to an HXR burst (*e.g.*, Temmer *et al.*, 2008). The plots calculated from the microwave burst lag behind the measured kinematical plots of the filament by about two minutes indicating that most likely the flare was caused by the eruption. This circumstance suggests that the eruptive filament accelerated almost independently of the flare reconnection rate and HXR emission, at least, in this event.

There are two options regarding a relation between the bright feature and the loop. One possibility is that $\approx 1.5-2$ minutes after the start of the acceleration of

the bright feature, the loop suddenly and independently underwent much higher impulsive acceleration. Alternatively, the loop was expelled by a shock front that appears to be more probable. For the latter case the strength of the shock can be estimated. The Mach number is $M = V_{\rm sh}/V_{\rm fast}$, where $V_{\rm sh}$ is a shock speed, and $V_{\rm fast}$ is a fast-mode speed. The shock speed $V_{\rm sh}$ at the onset of the loop motion can be roughly estimated from the power-law fit (Grechnev *et al.*, 2008) to be about 1000 km s^{-1}, but is rather uncertain because of insufficient temporal coverage by TRACE images and their long exposure times. The fast-mode speed can be estimated from an expression $V_{\rm sh} \approx V_{\rm fast} + \kappa U_{\rm sh}/2$, $(\gamma+1)/2 \leq \kappa \leq 3/2$, γ the polytropic index. We take the speed of the loop as a gas speed behind the shock front, $U_{\rm sh} \approx 320$ km s^{-1}. With these quantities and $\kappa \approx 3/2$ for the wave propagation perpendicular to the magnetic field, the Mach number is $M \approx 1.3$. One might suppose that the steepening time was about the interval between the peaks of the solid and dotted curves in Figure 4c that show acceleration profiles for the bright feature and the loop, *i.e.*, about 0.5 minutes.

We extrapolated magnetic fields into the corona using a package of Rudenko and Grechnev (1999) based on a potential approximation of Rudenko (2001). The result showed that the eruptive loop system was strongly inclined to the photosphere, and a height of the loop top was about 30 Mm. With a height of the pre-eruptive filament of > 10 Mm, the shock front hit the loop almost horizontally, and the estimated Mach number is related to the horizontal direction, while in the vertical direction the shock was probably stronger.

These results show that most likely the loop itself was passive, and its motion was driven by the shock wave. Grechnev *et al.* (2008) found that all observed products of the eruption monotonically decelerated starting from TRACE observations and up to LASCO/C3 ones. The loop therefore is unlikely to have excited the second shock wave, as PHS hypothesized.

3.1.2. Moreton/EUV Wave, Type II burst, and CME

Grechnev *et al.* (2008) could not find out from kinematics if the leading edge of a coronal transient observed by LASCO (see Figure 2b) was a mass ejection or a trace of a wave. However, comparison with a non-subtracted image of the corona before the CME in Figure 2c suggests that the spiky leading fringe of the transient was most likely due to deflections of coronal rays caused by a wave. This is especially pronounced for feature F1 at the position angle of 294°. Assuming the CME leading edge to be formed by the wave, we fitted the measurements from the CME Catalog by a power law with a known onset time of 00:14:50. As Figure 5 shows, the calculated curves with $\delta \approx 2.6$ corresponding to the Saito model agree with the measurements. The speeds computed from these height-time plots within the LASCO/C2 and C3 fields of view are in reasonable agreement with the linear-fit speeds, while the estimated speeds within the interval when the type II burst was observed are two to three times higher.

Now we try to fit the drift of the type II burst. Figure 6c presents the dynamic spectrum produced by the HiRAS radio spectrograph along with a power-law fit of both the fundamental and second-harmonic emission (solid lines). We used the density falloff index $\delta = 2.1$, close to the Newkirk model expected for a streamer.

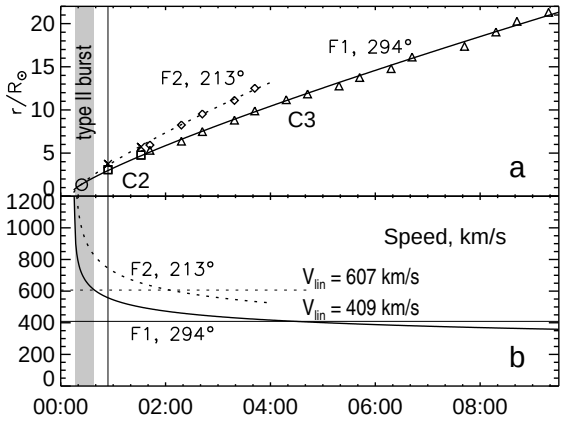

Figure 5. a) Measurements from the CME Catalog for the F1 and F2 CME components fitted with the shock-PL model, $\delta \approx 2.6$. The circle denotes the position of the off-limb EUV wave at 294°. b) Speed-time plots corresponding to each fit. Linear-fit speeds are also specified. Shading denotes the interval in which the type II burst was observed.

The QF1 and QF2 are features open to question; their presence hinted at two different shock waves. The dotted lines approximately reproduce the outline of PHS following the logic suggested by their Figs. 4 and 6, and correspond to fixed velocities of the type II exciters. However, a flare blast wave proposed by the authors is expected to decelerate.

The solid power-law fit satisfactorily outlines the whole slowly drifting structure even starting from the decimetric range and up to the lowest frequency. A question remains about features QF1 and QF2. The former feature was probably a disturbed type III emission as PHS identified, with an uncertain harmonic structure. It does not seem to favor the dotted outline with respect to the solid one. The weaker QF2 feature, which the authors considered as the onset of the second type II burst, indeed seems to have a harmonic structure and to start at about 00:23. To find out its probable nature, we show in the inset a portion of the spectrum recorded at the US Air Force RSTN Learmonth station with a higher spectral resolution. A pronounced (-like feature suggests an encounter of a shock wave with a dense structure (see Section 2.3). These facts support association of the type II burst with a single decelerating shock wave. The drifting continuum, which PHS found to start at 00:13 (confirmed by our acceleration profile in Figure 4f), might be due to emission from an expanding pre-shock region propagating upwards, towards a decreasing density or, alternatively, from inside of the expanding region with a progressively depleting density. PHS argued in favor of the latter option. Compression of the environment within the pre-shock interval from 00:13 to about 00:14:50 might produce an excessive plasma density, which we describe with a radial power-law falloff.

For comparison we also show in Figure 6a the distance-time measurements of the Moreton wave (triangles) and the EUV wave (open circles) from Grechnev *et al.* (2008) along with power-law plots for the three directions 1, 2, and 3 denoted in Figure 2a, and the dotted plot of a spherical weak shock in uniform plasma calculated by using expressions of Uralova and Uralov (1994). Figure 6b presents

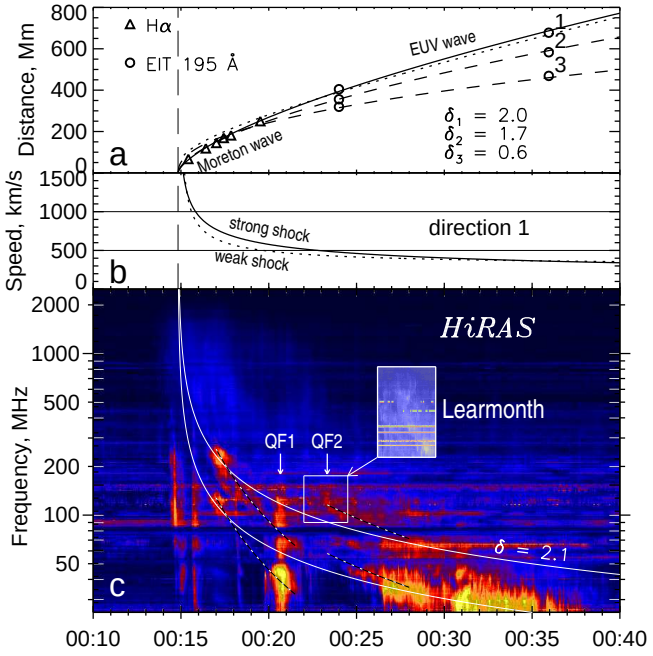

Figure 6. The 13 July 2004 event. Height-time (a) and velocity-time (b) plots of the Moreton and EUV waves, and (c) the fit of the type II burst ($\delta = 2.1$). Qf1 and QF2 are features open to question. A reverse drift of Qf2 is detectable in the inset which shows a portion of the dynamic spectrum recorded in Learmonth with a higher spectral resolution.

the speeds for the strong (solid) and weak (dotted) shock approximations along direction 1. Both approximations are close to each other far from the eruption center ($r \gtrsim R_1 \approx 200$ Mm) being different at shorter distances. The shock wave propagating along the surface probably became weak at $r \gtrsim R_1$, when it left the active region and entered quiet Sun's areas where the coronal plasma density and the fast-mode speed were nearly constant, *i.e.*, $\delta \to 0$. Closer to the eruption site ($r < R_1$) where the plasma density presumably had a power-law falloff, the shock was not weak, and the self-similar strong shock approximation applies.

Note that deceleration of the EUV wave which propagated over a quiet solar area was stronger towards the equator, as comparison of the three fronts in Figure 2a for the 1 – 3 directions shows. This is expected for a strong shock, whose deceleration is determined by the density distribution which has a maximum at the equator (see the Saito model). This is also expected for a weak shock, whose propagation is governed by the Alfvén velocity decreasing towards the equator due to both the density distribution and the dipole magnetic field of the Sun.

Our analysis of Event 1 has revealed a probable excitation of a single wave by an impulsively accelerated eruption and steepening into a shock within one minute. Then the wave freely propagated like a decelerating blast wave and probably formed the leading edge of the CME. Our results are coherent with the conclusions of PHS about the role of a rapidly expanding eruption, formation of the shock wave at a very low altitude, and their estimates of the shock speed.

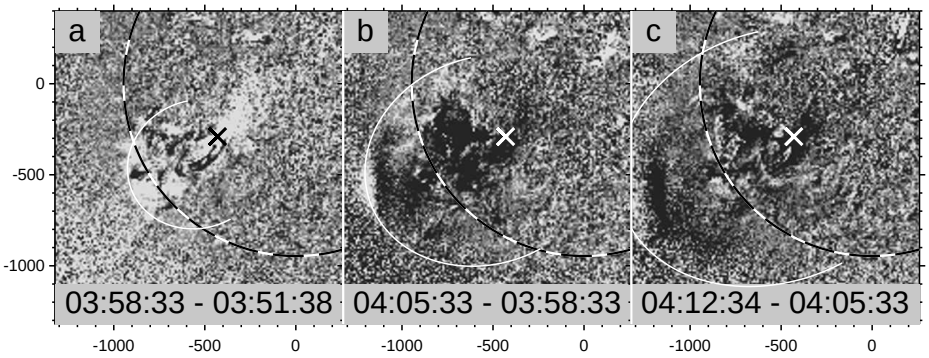

Figure 7. An EUV wave (outlined with ovals) on 1 June 2002 in EIT 195 Å running-difference images. The dashed circles denote the solar limb. The slanted cross marks the flare site.

3.2. Event 2: 1 June 2002

A possible coronal shock wave presumably excited by a collision of an eruptive magnetic flux rope with a magnetic obstacle was revealed by Meshalkina *et al.* (2009) in the 1 June 2002 event. An M1.5 flare (S19 E29) started at 03:50 and had a total duration of only 11 min. SOHO/EIT carried out the 'High cadence 195' program, and LASCO did not observe at that time. Figure 7 shows an EUV wave in this event to expand above the limb.

Figure 8a – f shows the eruption. Panels g – i present plane-of-sky kinematic measurements using the same technique as for Event 1. The eruption accelerated up to ≈ 7 km s^{-2} and then decelerated. The deceleration might be overestimated, because the eruption started to disintegrate and become transparent. Similarly to Event 1, the acceleration occurred during the rise of the HXR burst recorded with RHESSI, while the plasma pressure gradually increased all the time.

Figure 9 shows the kinematics of the EUV wave (a,b) and the dynamic spectrum of the type II burst (c) similarly to Figure 6. To reveal the harmonic structure of the burst, we use again the record made in Learmonth (the inset). The burst consisted of two pairs of emission lanes with frequency ratios in pairs of 2.0 and ≈ 1.5 between the pairs. This situation suggests propagation of the shock front along two streamers located close to each other. We accordingly outline the burst structure with two pairs of harmonically related power-laws, 1 and 2, with 'f' indicating the fundamental emission and 'h' the second harmonic. The difference in δ (2.4 and 2.6) might be due to differences of density falloffs in the streamers as well as different angles between the shock front and the axes of the streamers. The estimated onset time of the wave is 03:53:40, close to the time when the acceleration of the eruption was maximum (see Figure 8i).

In Figure 9a we also show the height-time plots for the type II exciters inferred from the fit of the dynamic spectrum in comparison with the off-limb EUV wave. Note that the type II emissions were observed when their sources were presumably located at heights from 190 Mm (heliocentric distance of $1.27R_\odot$) up to 500 – 600 Mm [$(1.7 - 1.9)R_\odot$], i.e., lower than usually assumed. Moreover, the fast-drifting decimetric continuum in this event is well fitted by the outline

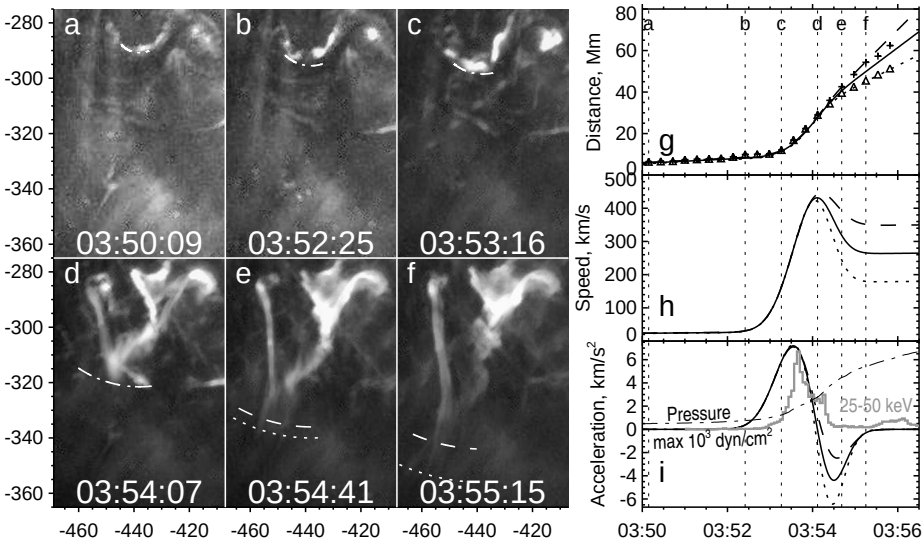

Figure 8. The eruption in TRACE 195 Å images (a – f) and measurements of its kinematics. The dotted and dashed lines correspond to different outlines of the eruption. Panel (i) also shows 25 – 50 keV time profile (gray) and pressure calculated from GOES data (dash-dotted).

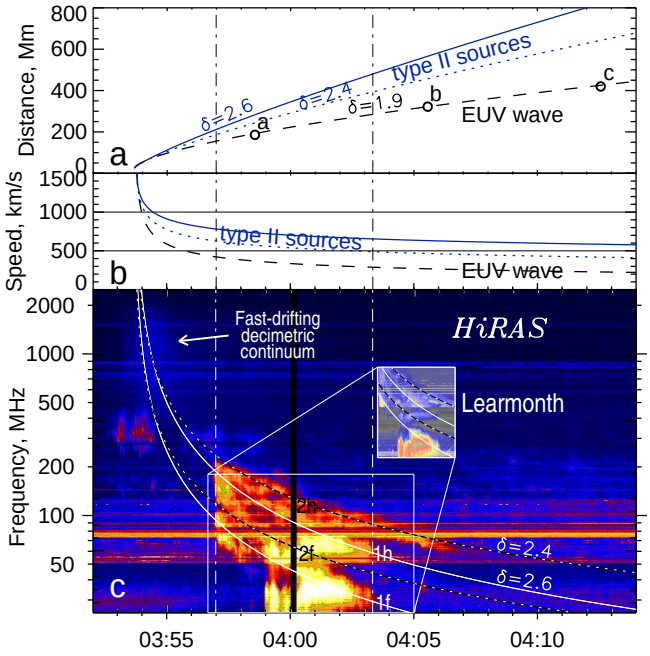

Figure 9. The 1 June 2002 event. Height-time (a) and velocity-time (b) plots of the EUV wave (dotted) and the fit of the type II burst source (solid). Open circles in panel (a) represent the distances of the foremost wave fronts from the eruption center, and labels 'a' – 'c' correspond to the images in Figure 7. Panel (c) shows a dynamic spectrum with a power-law fit. The vertical broken lines delimit the interval of the type II burst.

of the shock front suggesting its relation to the shock wave, which presumably appeared still lower. The type II burst probably started when the shock front reached the streamer and then ceased due to deceleration and fading of the wave.

3.3. Event 3: 19 May 2007

This event associated with a B9.5 flare at 12:48 – 13:19 (N07 W06) and a fast CME has been well studied due to efforts of several researches mostly from observations made with EUV Imager (EUVI) of SECCHI complex (Howard *et al.*, 2008) on STEREO (Kaiser *et al.*, 2008). Nevertheless, some questions remain.

Long *et al.* (2008) measured the kinematics of the EUV wave and found its pronounced deceleration. They established that the long-standing problem of low velocities of 'EIT waves' might be due to their temporal undersampling. They also concluded that the observations were consistent with an impulsively generated fast-mode magnetosonic wave or propagating MHD shock. However, they revealed an initial acceleration of the wave-like disturbance from a nearly zero velocity that does not seem to match this conclusion, because an MHD wave should not gradually accelerate starting from zero velocity.

Veronig, Temmer, and Vršnak (2008) also measured deceleration of this disturbance indicative of a freely propagating MHD wave and revealed a wave reflection at a coronal hole. They assumed that the wave was initiated by the CME expanding flanks and noticed that the associated flare was very weak and occurred too late to account for the wave initiation. They also revealed two eruptions following each other within nine minutes.

Gopalswamy *et al.* (2009) measured propagation of wave fronts reflected in different directions and considered the reflections as an argument in favor of a wave nature of EUV transients. Schmidt and Ofman (2010) successfully simulated the reflected waves in this event thus reinforcing the above conclusions.

However, Attrill (2010) proposed that the reflections were actually illusions resulted from a misinterpretation of the running difference data and suggested instead that two coronal wave fronts actually developed during the eruption. Indeed, running differences reliably show only the outermost boundary of an expanding disturbance, while the inner picture reflects all changes, which occurred between two images subjected to subtraction (Chertok and Grechnev, 2005).

To understand whether or not the reflections actually occurred, we firstly look at a movie composed of non-subtracted images of STEREO-A/EUVI 171 Å ('euvi_ahead_171.gif' in the electronic version of the paper). A backward northeast motion from a plage region denoted in Figure 10a is visible after 13:11 suggesting a reflection. Then we repeated the measurements of Gopalswamy *et al.* (2009), but without any subtraction. Due to a complex character of the event and difficulties to reveal wave fronts in non-subtracted images, we only consider the first probable reflection in the direction exactly backwards. Figure 10 corresponds to Figures 1 and 2 from their paper. To enhance the sensitivity, instead of slices selected from images as panel (a) shows, we use in panel (b) spatial profiles computed as the sums over the width of each slice. Each image was normalized to a single pre-event image taken at 12:16:30 (fixed-base ratios).

Figure 10b shows that after arrival of the wave front, the plage region 'sagged' and then returned back. A backwards motion from plage A is faintly visible after

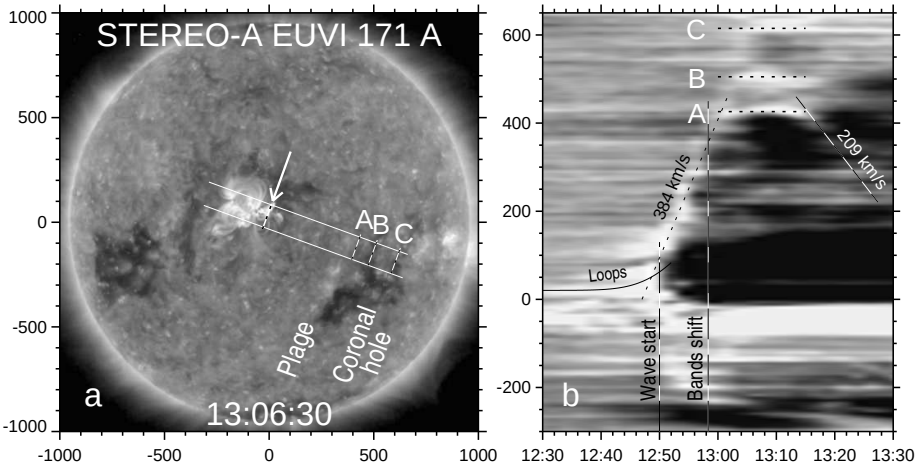

Figure 10. EUV wave observed with STEREO-A/EUVI at 171 Å on 19 May 2007. Spatial profiles (b) computed from ratio images within the strip denoted in panel (a). The arrow points at the origin of measurements. The A, B, and C broken bars in both panels mark the reflection positions. The thin inclined broken lines in panel (b) outline the steepest slopes.

13:14. Region B exhibited a weaker sag. It is not clear if the wave was reflected from the A or B region; the latter seems to be preferable because continuations of both the direct and reflected slanted traces intersect farther from region A, while a prolonged standing of the wave at region A is doubtful. The slanted broken lines show the speeds found by Gopalswamy *et al.* (2009) and agree with the slopes in Figure 10b. We conclude that the results of the authors were correct, at least, for the first reflection. The wave reflected backwards was significantly slower than the incident wave. This feature supports a shock-wave nature of the disturbance. Indeed, if an incident shock wave propagating with a velocity $V_{\rm inc\ sh}$ encounters a semitransparent "wall" like a coronal hole, then the shock reflected backwards is slower: $V_{\rm back\ sh} \approx V_{\rm inc\ sh} - V_{\rm gas}$, where $V_{\rm gas}$ is a velocity of the gas trailing the shock front. It can be up to the sound speed.

The second question is what does the accelerating part prior to 12:50 display. Figure 11 shows EUVI-A 171 Å images without subtraction in the upper raw and fixed-base differences in the lower row. The outermost boundary of the expanding bright feature coincides with the edge of coronal loops visible in the earlier non-subtracted images. Then eruptive loops rapidly loose brightness due to expansion and become invisible in non-subtracted images. We conclude that the accelerating part measured by Long *et al.* (2008) was related to the expanding magnetic loops (a future CME), while the decelerating part was related to the wave. It is very difficult to recognize an appearing decelerating wave, which brightens, and an accelerating piston (loops), which becomes transparent. For this reason the acceleration of the loops is uncertain within $120 - 270$ m s^{-2}; the outline in Figures 10 and 11 corresponds to 260 m s^{-2}.

Figure 12a shows the detailed measurements of the wave presented by Veronig, Temmer, and Vršnak (2008) and their shock-PL fit (thick blue curve). The wave start (12:50) corresponds to the early rise phase of the HXR burst (red

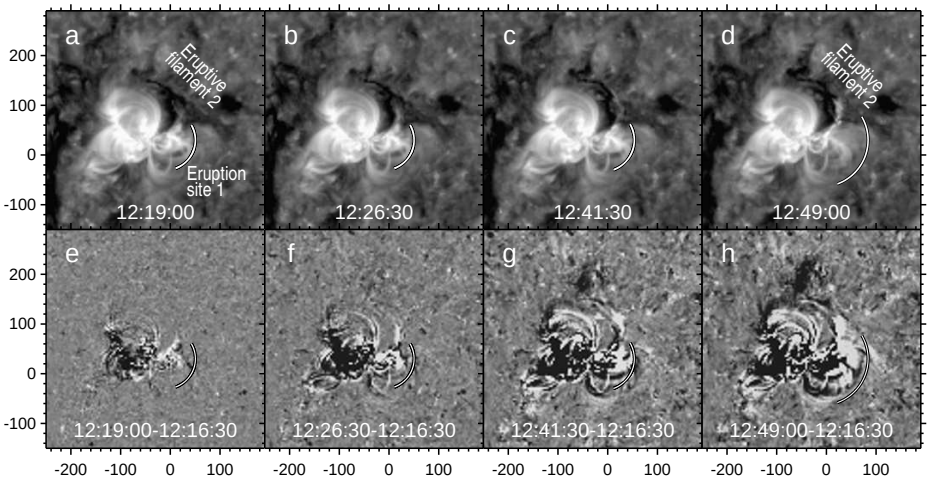

Figure 11. The first eruption on 19 May 2007 observed with STEREO-A/EUVI 171 Å. Top: non-subtracted images, bottom: fixed-base differences. The dashed arcs outline the foremost edge of the eruptive loop system according to the fit shown with the solid line in Figure 10b.

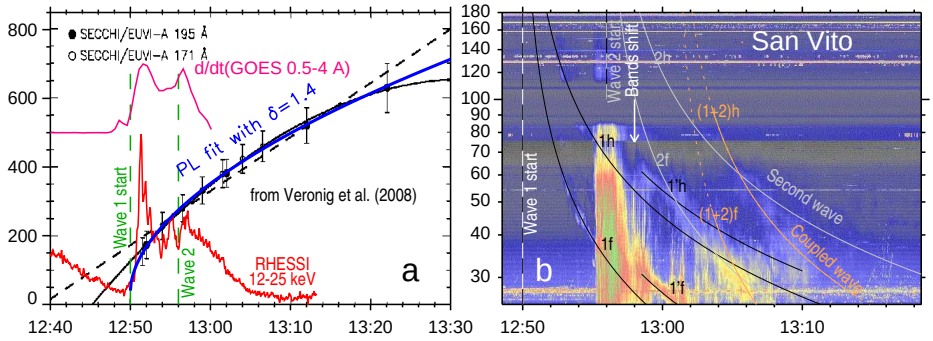

Figure 12. The 19 May 2007 event. a) Propagation of the EUV wave measured by Veronig, Temmer, and Vršnak (2008) (black) along with an HXR time profile (red), a derivative of the SXR flux (pink), and a shock-PL fit (blue). b) Dynamic spectrum of the type II burst with four pairs of bands shock-PL-fitted ('f' fundamental emission, 'h' second harmonic). Matching bands are shown with the same line styles. See details in the text.

in Figure 12a, also from their paper), and the power-law fit corresponds to the measurements of the authors better than their quadratic and linear fits based on a constant and zero accelerations. Again the eruption accelerated before the appearance of pronounced flare reconnection manifestations.

The suggestion of Attrill (2010) about the second wave appears to be correct. Both TRACE and EUVI show that the second eruption was probably triggered by the first one. Activation of filament 2 started at about 12:47, and its eruption occurred at 12:55 – 12:57 according to TRACE 173 Å images. The HXR time profile was complex, but the two distinct episodes are detectable in the derivative of the SXR flux recorded with GOES (pink in Figure 12a). The onset times of the two waves were about 12:50 and 12:56.

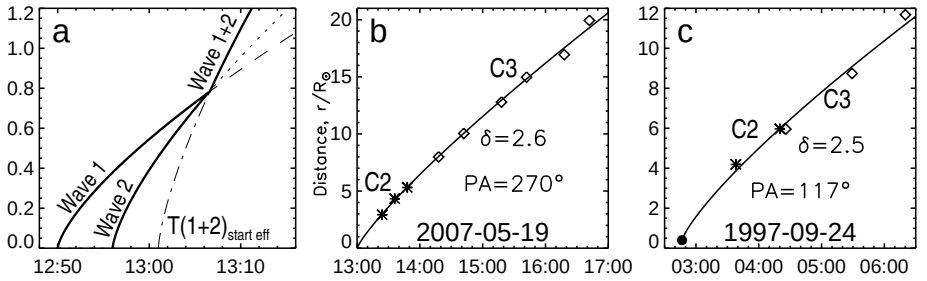

Figure 13. Coalescence of two shock waves (a) and height-time plots of CMEs observed on 19 May 2007 (b) and 24 September 1997 (c). Symbols present data from the CME Catalog, lines show their shock-PL fit. The filled circle in panel (c) denotes the origin of the wave.

The second wave following the first one propagates in a decreased plasma density swept up by the leading front and can reach it. In such a case, the two shock waves coalesce to produce a single shock front (and a weak backwards disturbance, which we are not interested in). Its speed is less then the sum of the initial fronts' speeds; nevertheless, the resulting shock is stronger and faster than either of the initial ones. The slope of its distance-time plot is accordingly steeper than the initial waves had, and its virtual onset time is later than either of initial waves, as schematically shown in Figure 13a.

Let us try to understand a complex dynamic spectrum in Figure 12b recorded in San Vito (USAF RSTN). We do not consider a type III emission at 12:55 – 12:58. A harmonic pair of rather weak lanes 1f, 1h is sometimes detectable after 12:52. Two stronger lanes 1'f, 1'h appear at 12:58 resembling an inverse-N-like shift of the initial bands suggesting that a part of the shock front entered a denser region. The initial 1f, 1h lanes are still detectable sometimes. The outline of both these pairs of lanes has the same start time of the first wave, 12:50. The appearance of the second pair might be due to the entrance of the shock front into a dense region located rather high above plage A (see Figure 10a,b). The surface EUV wave reaches plage A slightly later, as expected for a convex front.

The second shock front was probably manifest in weak 2f, 2h lanes (pale, the start time is 12:56). Lanes denoted (1+2)f and (1+2)h (orange outline) probably reveal the resulting shock with a virtual start time of 13:01. All of these lanes overlap with others increasing the total emission at the intersections. We remind that various lanes were most likely emitted from spatially different sites.

The CME Catalog shows that the corresponding CME measured at a position angle of 270° was fast (958 km s^{-1}) and decelerated. We assume again that the CME leading edge was a trace of a wave, and apply a shock-PL fit to the measurements from the CME Catalog (Figure 13b). The onset corresponds to the virtual start time of the coupled shock wave, and the density falloff corresponds to the Saito model. A trailing CME centered at 310° and probably related to the same event was significantly slower (294 km s^{-1}) and poorly observed. Its estimated deceleration might be due to both the influence of the wave running ahead and difficulties of measurements.

These considerations do not pretend to be perfectly true, but they nevertheless show that even such a complex dynamic spectrum can be reconciled with EUV

observations and the CME propagation under assumption of the shock-wave nature of the related disturbances. But some questions still remain. For example, it is not clear if the higher velocities measured by Gopalswamy *et al.* (2009) for the fronts, which presumably passed through the coronal holes and turned north, with respect to the incident front were due to a higher fast-mode speed in a coronal hole or the coalescence of two shock waves. The event was really very complex, and oversimplified considerations can be misleading. In particular, Yang and Chen (2010) concluded that the EUV wave speed in this event was less in regions of stronger magnetic field that appeared to be a challenge for the wave hypothesis. However, 1) the authors considered the radial component of the magnetic field only, whereas the Alfvén speed is known to depend on its magnitude. 2) By taking the range of the magnetic field strengths ≤ 0.6 G, for which Yang and Chen obtained anticorrelation with the EUV wave speed, and a density of $\gtrsim 2{\times}10^8$ cm^{-3} from the Saito model, one obtains $\beta = (2/\gamma)C_{\rm s}^2/V_{\rm A}^2 \gtrsim 4$, which means that the wave was insensitive to the magnetic field. 3) The fronts in their Figure 4 stretched west-southwest and became sharply pointed at 12:59, whereas Long *et al.* (2008), Veronig, Temmer, and Vršnak (2008), and Attrill (2010) all independently showed the front to be blunt in this direction at that time. 4) The usage of the Huygens plotting technique to find trajectories of the wave front resulted in a strange picture of intermittently condensed and rarefied ray trajectories in their Figure 4. Thus, the results of Yang and Chen (2010) do not appear to offer problems for the shock-wave hypothesis.

3.4. Event 4: 24 September 1997

This event was associated with a short M5.9 flare (02:43 – 02:52, S31 E19). A Moreton wave and EUV wave observed in this event were first presented and analyzed by Thompson *et al.* (2000). Warmuth *et al.* (2004a, 2004b) established the kinematical closeness of both wave fronts to each other and their common deceleration. The first EUV wave front (Figure 14a) was unusually sharp and bright suggesting that the main EUV-emitting layer was low. A running difference divided by a pre-event image (panel b) reveals weak wave manifestations south, southwest, and slightly west from the outline of Warmuth *et al.* (2004a). The third front in panel c is close to their outline. The deceleration of the EUV wave was therefore even slightly stronger than the authors estimated.

White and Thompson (2005) analyzed wave signatures in microwave images at 17 GHz but did not reveal any deceleration. Their other important conclusions were: *i*) the speed of the microwave disturbance was 830 km s^{-1} against $\approx$ 500 km s^{-1} estimated for the Moreton wave; *ii*) the brightness temperature at 17 GHz was about five times higher than an estimate from EIT data, and the discrepancy could be reduced if (a) the dominant kinetic temperature at 17 GHz would be different (preferentially higher) from the characteristic temperature of the 195 Å channel or (b) photospheric rather coronal abundances were assumed. The authors also concluded that the timing of images should be corrected by ≈ 100 s for EIT and by ~ 180 s for Hα to reconcile all observations.

These facts and our considerations indicate that the layers emitting microwaves and EUV were not identical. Indeed, the higher speed, lesser decel-

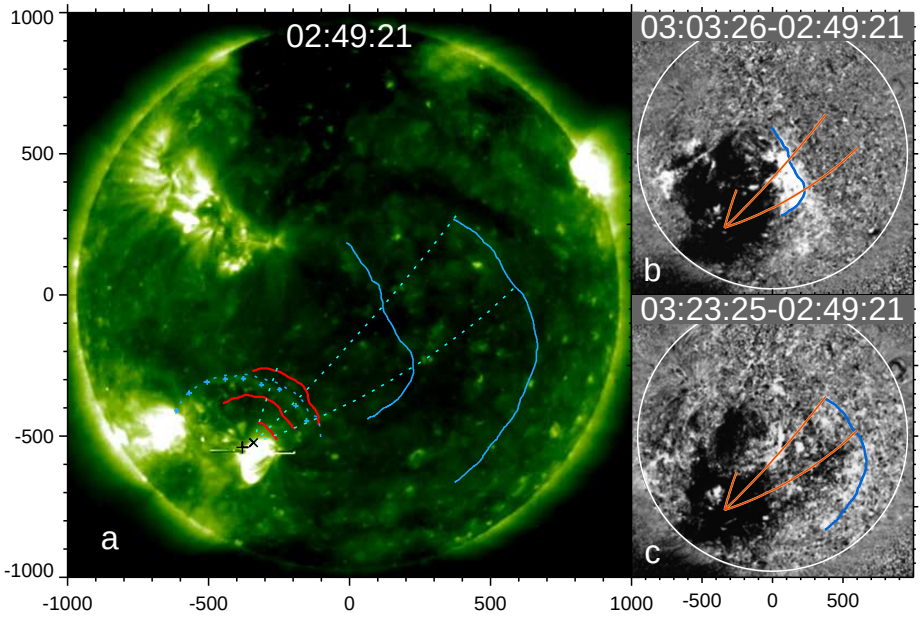

Figure 14. EUV wave (blue) and Moreton wave in the 24 September 1997 event. a) Non-subtracted EIT 195 Å image with the first sharp front denoted with blue crosses. The blue dotted line outlines its faint foremost edge. The red fronts outline the Moreton wave, and the broken lines denote measurement great circles. The black crosses denote the origins of measurements. b,c) Difference ratio images with blue outlines of EUV wave fronts and red measurement great circles. The outlines of the wave fronts and the great circles correspond to those in Warmuth *et al.*, 2004a (courtesy A. Warmuth). The nominal corrected times are specified for EIT images.

eration, and higher brightness temperature (*i.e.*, column emission measure) observed at 17 GHz with respect to EUV hint at a possibly higher location of the microwave-emitting layer. Figure 15 shows our suggestion in panel (c), and panel (a) presents the distance-time plots from both papers. The corrected times of EIT images (+99 s) and Hα ones (+170 s) are specified at data points.

To reconcile the kinematics of the microwave and EUV/Moreton wave fronts in a simplest way, we shift the White and Thompson data by 40 Mm and fit the two data sets with the same start time of 02:46:50 but different power-laws. A cartoon in panel (c) explains the idea: the lower part of the front propagating in high-density regions decelerated stronger ($\delta \approx 2.3$ from Warmuth *et al.* measurements), while microwaves were dominated by long cross sections of the wave front (bars 1 – 4) running in lower-density regions, $\delta \approx 2.8$ (*cf.* Paper III). The large-height EUV wave's leading edge detectable close to the eruption center diminished at large distances, where the EUV wave was dominated by low structures. The wave presumably appeared at a significant height (the star). With a difference between the origins of measurements (black crosses in Figure 14a) of ≈ 32 Mm and our shift of 40 Mm, assuming spherical wave fronts, we get a height of 117 Mm. It seems to be overestimated; an estimate of about 75 Mm from the dynamic spectrum appears to be more plausible. The overestimate implies that

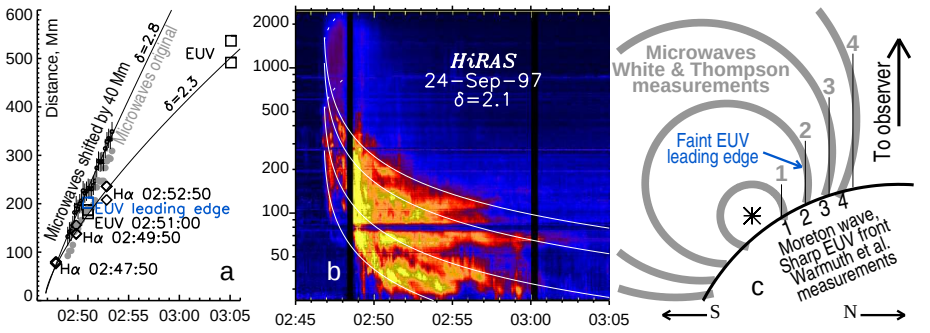

Figure 15. a) Propagation of the EUV wave (squares) and the Moreton wave (diamonds) measured by Warmuth *et al.* (2004a). Filled gray circles represent the measurements of White and Thompson (2005), and black open circles with error bars show them shifted by 40 Mm to match common kinematics. Both data sets are outlined with shock-PL fit. b) The HiRAS dynamic spectrum outlined with shock-PL fit. The dotted outline indicates the negatively drifting continuum. c) A presumable relation between microwave-emitting and EUV/Hα-emitting layers. The thin vertical lines show cross sections of the wave fronts of the largest column emission measure presumably contributing 17 GHz emission. The star denotes the wave origin.

the wave could be strongly anisotropic starting from its appearance, or the wave exciter was large (the wave origin should be shifted north), or both.

A dynamic spectrum shown in panel (b) was complex, with emissions at higher harmonics and an inverse-N-like shift of bands. The details are indiscernible in the figure, and we do not discuss them. We have outlined the harmonic numbers of 1, 2, and 4; the highest-frequency envelope of the burst has been formally outlined as the sixth harmonic. The outline corresponds to the initial height of 75 Mm, the same wave start time of 02:46:50, and $\delta \approx 2.1$ typical of streamers. A negatively drifting continuum (broken outline) at the initial stage of the burst indicates propagation of the shock front towards the chromosphere.

A poorly observed CME centered at 137° with a speed of 531 km s^{-1} was injected into a preceding CME. The CME Catalog estimates its acceleration to be positive with a remark about uncertainty. By adding the known origin of the wave (the filled circle in Figure 13c), we get a shock-PL fit of the measurements from the CME Catalog with an index typical of the Saito model.

Our considerations confirm correctness of the results of both Warmuth *et al.* (2004a) and White and Thompson (2005), reconcile these results with each other and with parameters of the type II burst as well as the CME by taking account of properties of shock waves. The deceleration of the front portion detectable in microwaves was significantly less than its lowest part visible in EUV and Hα had. Hence, it was not possible to reveal deceleration from microwave observations, which allowed detection of the wave within an interval as short as 4.5 min.

4. Discussion

TRACE observations of abrupt eruptions in events 1 and 2 (with imaging intervals of 40 – 60 s and 17 s, respectively) have revealed accelerations of magnetic rope structures of 4 – 7 km s^{-2}, *i.e.*, (15 – 25)-fold gravity acceleration in the plane

of the sky. Then the eruptions underwent significant decelerations in both these events. Coronal waves appeared in events 1 – 3 approximately at the maximum of the acceleration. The onsets of the waves in all four events corresponded to the rise phases of HXR or microwave bursts (in event 4 according to White and Thompson, 2005). We roughly estimated that the wave in event 1 steepened into a shock within one minute and reached a Mach number of about 1.3 in a horizontal direction, while the upwards shock could be stronger. In the next Section we consider which of known shock formation scenarios (see, *e.g.*, Vršnak and Cliver, 2008) appear to match the observations.

4.1. Comparison of Observations with Shock Formation Scenarios

A scenario in which a coronal shock is formed by a gas pressure pulse generated in a flare is based on an idea that the β ratio of the coronal plasma pressure to the magnetic pressure sharply changes from $\beta \ll 1$ to β significantly exceeding unity. Such a change of β is believed to be possible in a flare loop and considered as a cause of a wave disturbance propagating omnidirectionally. Dramatic changes of the volume of a loop or its abrupt motion are necessary to get a significant intensity of a wave excited in this way. Objections against this scenario do exist.

1) As Grechnev *et al.* (2006a) showed, the effect of a high β (even $\beta > 1$) in a flare loop is not dramatic, only an increase of all its linear sizes as small as $\sqrt[4]{1+\beta}$. 2) An assumption that a situation of $\beta \to 1$ can result in instability of a loop is not confirmed by observations. For example, Ichimoto, Sakurai *et al.* (1993) and later Grechnev *et al.* (2006b) concluded that the $\beta < 1$ condition was not satisfied in long-lived coronal loops visible in soft X-rays. 3) The time profiles of the flare pressure in events 1 and 2 were gradual, without any marks of the wave appearance. 4) The sizes of the SXR-emitting regions found from RHESSI data in events 1 and 2 did not show any changes during the intervals in question, when the pressure increased. Veronig, Temmer, and Vršnak (2008) also concluded that the wave initiation in event 3 by the flare pressure pulse was unlikely. All these facts make the ignition of waves by flares doubtful. Note that a slower motion of the main body of a CME well after a shock front does not provide an alibi for a CME: as events 1 and 2 demonstrated, eruptions responsible for the wave excitation can significantly decelerate and mimic a situation as they were not implicated (*cf.* Magdalenić *et al.*, 2008, 2010).

The maximum plane-of-sky speeds measured for the eruptions in events 1 – 3 appear to be significantly less than the Alfvén speed expected at moderate heights (< 100 Mm) above active regions (see, *e.g.*, Mann *et al.*, 2003), where the waves appeared. Corrections due to off-plane orientations are insufficient. The time profiles of the speeds estimated for the eruptions and waves were quite different. For these reasons, the bow shock scenario is also unlikely.

4.2. Impulsive Piston Scenario

In a simplest scheme of this scenario, a piston moving with a speed U undergoes an impulsive Π-shaped acceleration of a value and zero both initially and finally. An important condition is that the piston extrudes plasma, *i.e.*, plasma cannot flow around the piston (this occurs, *e.g.*, in a three-dimensional expansion

of an arcade). In a flat geometry and homogeneous medium the plasma flow ahead of the piston corresponds to a simple wave. The discontinuity appears at $t^0_{\rm sh} = V_{\rm fast}/(\kappa a)$ at a distance $r^0_{\rm sh} = V_{\rm fast} t^0_{\rm sh}$ with $(\gamma + 1)/2 \le \kappa \le 3/2$ that is quite similar to a solution of an analogous gas-dynamic problem (Landau and Lifshits, 1987). Then the speed jump in the discontinuity increases up to the piston's maximum speed, $U_{\rm max}$. The condition $U > V_{\rm fast}$ essential for a bow shock formation is unnecessary in the impulsive piston scenario.

The accelerations and their durations before the appearance of the waves estimated in Section 3 are as follows: 4 km s^{-2} and 90 s in event 1; 7 km s^{-2} and 70 s in event 2; $0.12 - 0.27$ km s^{-2} and 800 s in event 3. Indeed, the stronger acceleration, the faster a shock appeared.

Observations indicate that the coronal shock waves in the four events were most likely excited by eruptive magnetic rope structures as impulsive pistons, which one might call the appearing CMEs. Then the waves rapidly steepened into shocks, detached the pistons, and freely propagated afterwards like blast waves. The shock excitation mechanism implies a source height to be nonzero, but rather low in the corona, presumably < 100 Mm, as suggested by all dynamic radio spectra and implied by observations of event 4. The shock character of the waves is supported by the close correspondence of their kinematics to the expected propagation of shock waves as well as the observed drift rates of type II bursts and fast-drifting continua. The shock-wave nature of EUV waves is also supported with reflections and coupling of two shock waves, which, most likely, indeed occurred in event 3. Furthermore, expansion of leading edges of CMEs produced in these events corresponded to the propagation of the lower skirts of the shock fronts observed as Moreton/EUV waves. Thus, the wave excitation by an impulsive ('temporary') piston appears to match all the considered observations and basically corresponds to a picture proposed by Uchida (1974).

The fact that the measured speeds of the pistons were less than those required to produce the wave speeds estimated in terms of our shock-PL approach might be due to the following reasons. (1) The temperature sensitivity ranges of EUV channels which we used could be insufficient to catch the fastest parts of the eruptions, while heating at their fronts was quite possible. (2) Our approximation has a weakness close to the wave origin, where both the power-law density model and the initial speed of the wave infinitely increase (see 2.1). However, the fact that the shock-PL description closely matches the drift rates of radio bursts up to decimeters indicates that our approximation correctly reproduces a relation between real plasma density distributions and wave velocities.

While talking about a piston, we did not relate it so far with a particular magnetoplasma structure or its surface. Presumable pistons could be either an eruptive filament (EF) or a CME frontal structure (FS). Both these structures expand as an entire ensemble in a completely formed CME, and the role of a piston can only play its outer sheath, which is believed to be both the surface of contact discontinuity and the outer surface of the frontal structure. The motion of such an FS-piston determines propagation of an interplanetary piston-driven wave and accordingly the drag force affecting a CME. A different situation is possible during the early CME formation inside an active region, when an eruptive filament writhes and expands faster than it would be necessary to establish

a self-similar expansion regime of the whole CME. The eruptive filament acts in this situation as an impulsive piston and excites inside an appearing CME a wave, which freely propagates outwards as a shock wave. In the four events considered in Section 3 we revealed just this excitation scenario of waves, which resembled blast ones. Propagating upwards, such a wave inevitably would pass through the frontal structure and appear ahead of it.

4.3. Magnetoplasma CME Components and Waves

Expansion of a magnetoplasma CME's constituent is different from the kinematics of a wave traced, *e.g.*, with a leading edge of a plasma flow driven by a shock. The CME expansion is known to be about self-similar at moderate distances from the Sun. *Note that the self-similar approach does not apply to early stages of an eruption, when the structure and shape of a CME have not yet established.* When an MHD instability driving an eruption completes, and the aerodynamic influence of the solar wind is not yet significant, the self-similar CME kinematics can be obtained from considerations of forces applied to the CME. This problem was first solved by Low (1982), and later Uralov, Grechnev, and Hudson (2005) obtained expressions, which were convenient in handling observational data.

Expansion of magnetoplasma structures is governed by magnetic forces, plasma pressure, and gravity as long as the effect of the solar wind is small. With the polytropic index $\gamma \approx 4/3$ all the forces integrated over the boundary and volume of a CME scale with distance r from the expansion center by the same factor of r^{-2}. This leads to an expression for the CME velocity $V_{\rm CME}^2 = V_0^2 + (V_\infty^2 - V_0^2)(1 - R_0/r)$, $V_{\rm CME} = dr/dt$ (Grechnev *et al.*, 2008). Here R_0 is the initial size of self-similar expansion, V_0 the initial velocity at R_0, and V_∞ the asymptotic velocity in infinity. At large distances the acceleration goes $\propto r^{-2} \rightarrow 0$ and $V_{\rm CME} \rightarrow V_\infty$. Since expansion of the CME frontal structure starts practically from a static equilibrium, most likely, the FS does not decelerate at the self-similar stage. An FS-piston either accelerates or moves with a nearly constant speed at this stage. By contrast, shock waves in all considered events decelerated. Hence, an FS-piston is expected to eventually approach the wave front.

What does such a relation between the speeds of the shock front and piston mean? Does a solution of MHD equations exist that would allow a decelerating shock wave to run for a long time ahead of a non-decelerating FS-piston? Answers can be found from a theory used by Low (1984) in solving a problem of self-similar expansion of a CME preceded by a strong shock wave. Although the problem could only be solved in an exotic limit of a very strong shock propagating in plasma with a too steep density falloff ($\sim r^{-26/7}$), the solution correctly shows a relation between accelerations of the FS-piston and a piston-driven shock. In solving such a problem important is an assumption of a common linear profile of the plasma velocity in the whole region of the motion, from the expansion center of a CME up to the shock front. Using this assumption alone, it is possible without a complete solution of the problem to obtain an expression relating acceleration of the shock front with acceleration, speed, and the position of the contact discontinuity, which we identify with the FS-piston. Then, by fitting the motion of the FS-piston with power-law functions in a form

$r_{\rm piston} = bt^m$, it is possible to express the sign of the shock front acceleration, $a_{\rm sh}$, versus m: $a_{\rm sh} \propto (\alpha m - 1)t^{\alpha m - 2}$ with $\alpha = (\gamma + 1)/2$. This expression shows that the conditions $a_{\rm sh} < 0$ and $a_{\rm piston} = d^2 r_{\rm piston}/dt^2 > 0$ are incompatible. Expansions of such an FS-piston and the shock front are inconsistent unlike a piston-driven shock. Consequently, a shock wave excited by an impulsive filament eruption and then freely propagating like a blast wave should eventually change to a piston-driven mode. Presumably this typically occurs at large distances, probably beyond the LASCO/C3 field of view. The transformation of a blast shock wave into a piston-driven one marks switch-on the aerodynamic drag and termination of the self-similar regime of the CME expansion. The drag force (which is not a 'self-similar' one) becomes significant that means establishment of a continuous energy transport from the FS-piston to the shock wave. Contrary to this situation, a blast-like wave excited by an eruptive filament and running ahead of a frontal structure, which does not yet act as a piston, facilitates expansion of a CME into solar wind. In this case, the shock wave forwards a part of its energy to the FS-piston, and the drag force is absent.

Real shock waves which we are dealing with, most likely, are neither purely blast waves nor purely piston ones. Indeed, the shock front is sensitive to any events occurring behind it, *e.g.*, changes of the FS-piston speed, because the fast-mode speed behind the shock front is higher than its phase speed. To produce one more shock wave, an FS-piston has to repeat the maneuver, which produced the first shock. This appears to be improbable when an MHD instability driving an eruption has completed and the CME left the Sun.

We also remind that the conic bow-shock shape is not expected, at least, for a wide CME. The shock front should cling to its foremost edge and closest flanks, while far flanks and a rear part can be constituted by a freely propagating shock front, so that the shape of the whole front would resemble an egg.

4.4. Presumable Scenario

The observations addressed in this paper and our considerations suggest the following presumable scenario of a flare-related eruptive event and a subsequent story. An eruption occurs due to a rapid development of an MHD instability of a magnetic rope structure (*e.g.*, a filament). An abruptly accelerating (on the order of a few hundreds m s^{-2} to a few km s^{-2}) eruption, on the one hand, destroys a pre-existing magnetic configuration, thus causing a flare, and, on the other hand, produces an MHD disturbance as an impulsive piston. The disturbance appears at a height of ~ 50 Mm during the rise phase of an HXR/microwave burst, leaves the piston, rapidly steepens into a shock wave, and then freely propagates like a blast wave. A trail of such a shock wave in the lower corona to the chromosphere might be observed as a decelerating Moreton wave as well as an EUV wave, and the dome of the wave front is sometimes observed to expand above the limb.

The upwards (and sometimes downwards) motion of the shock front can be manifest in dynamic radio spectra as a drifting continuum and, when the shock front reaches the current sheet of a coronal streamer, as a type II burst. According to observations, for the fundamental emission this usually occurs at ~ 100 MHz ($r \sim 1.5 R_\odot$ or $h \sim 350$ Mm). Metric type II bursts are expected to

cease due to damping of decelerating shock waves that occurs typically above 20 MHz, or $r < 3R_\odot$. Revival of a shock is possible at a few $R_\odot$ due to the decrease of the Alfvén speed. In such a case, decametric/hectometric (DH) type II emission can appear. The complex piston-blast-piston transformations of shock waves traveling in the corona with significantly varying parameters and possible coupling of multiple shocks imply well-known disaccord between metric and interplanetary type II events (*e.g.*, Cane and Erickson, 2005).

Expanding shock wave fronts can be seen as faint outermost envelopes of CMEs. Measurements in the CME Catalog refer to a fastest feature and for fast decelerating CMEs, especially halos, might be related to waves. Flanks and the rear of an egg-shaped shock front can be detected from deflections and kinks of coronal rays. Since a shock wave decelerates, a trailing mass ejection should eventually approach its front. The shock becomes a piston-driven one presumably at distances $r > 20R_\odot$. The aerodynamic drag becomes important afterwards.

This picture is consistent with results of, *e.g.*, Sheeley, Hakala, and Wang (2000), Warmuth *et al.* (2001), Khan and Aurass (2002), Gallagher, Lawrence, and Dennis (2003), Vourlidas *et al.* (2003), Cliver *et al.* (2004), Warmuth *et al.* (2004a), Pomoell, Vainio, and Kissmann (2008), Temmer *et al.* (2008), and other studies. The story of shock waves associated with flare-related CMEs appears to be more complex than often assumed, in fact combining different scenarios.

5. Concluding remarks

Our seemingly simplified approach has resulted in surprisingly fine reconciliation of EUV waves, Moreton waves, metric type II bursts with drifting continua up to decimeters, and leading edges of CMEs. The first consequence is that independent of the quality of our approximation, all these phenomena are really manifestations of a common agent, *i.e.*, a traveling coronal shock wave excited by an eruption. Second, our approach indeed appears to be a simple, convenient and efficient instrument for analyses of type II bursts and accompanying drifting continua and their comparison with other eruption-related phenomena. Our results clarify relations between flares, traveling coronal shocks, CMEs, related wave-like manifestations, type II bursts, and provide a common quantitative description for some of these phenomena. An important by-product of our analysis revealed from detailed observations is an indication of the leading role of eruptions with respect to flare development, *i.e.*, that the acceleration of an eruption occurs almost independently of the flare reconnection rate.

We glanced at some other events and succeeded in reconciliation of type II bursts with EUV waves in a few events, but not in all cases, because the picture was sometimes very complex and ambiguous. Consequently, the analysis, which we began, should be continued and extended, and the approach should be elaborated. A number of issues still needs addressing. Data sets similar to those analyzed in our paper should be compared with imaging observations in the metric range. The analysis of decimetric to metric drifting bursts, primarily type II emissions, should be extended to the dekametric/hectometric ranges in conjunction with coronagraphic observations. Despite success of our self-similar

strong shock approximation, a more realistic weak shock approximation should be considered. The last issue is a subject of our Paper II.

Acknowledgements We thank A. Warmuth for materials which he kindly made available to us. We thank him and M. Eselevich, E. Ivanov, E. Schmahl, V. Eselevich, A. Altyntsev, G. Rudenko, L. Kashapova, V. Fainshtein, N. Prestage, S. Pohjolainen, S. White, A. Zhukov, and J. Magdalenić for fruitful discussions and cooperation. We gratefully remember Mukul Kundu who inspired a significant part of our study.

We thank the teams operating all instruments whose data are used in our study for their efforts and open data policies: the ESA & NASA SOHO/EIT & LASCO, TRACE, and STEREO/SECCHI telescopes; the NOAA/SEC GOES satellites; the NICT HIRAS (Japan), the IPS Radio and Space Services Learmonth Observatory (Australia), and the USAF RSTN radio telescopes. We appreciatively use the CME catalog generated and maintained at the CDAW Data Center by NASA and the Catholic University of America in cooperation with the Naval Research Laboratory.

This research was supported by the Russian Foundation of Basic Research under grants 09-02-00115, 11–02–00038, and 11–02–00050.

References

Afanasyev, An. N., Uralov, A. M.: 2010, *Solar Phys.* Submitted.
Attrill, G. D. R.: 2010, *Astrophys. J.* **718**, 494.
Biesecker, D. A., Myers, D. C., Thompson, B. J., Hammer, D. M., Vourlidas, A.: 2002, *Astrophys. J.* **569**, 1009.
Brueckner, G. E, Howard, R. A., Koomen, M. J., Korendyke, C. M., Michels, D. J., Moses, J. D., *et al.*: 1995, *Solar Phys.* **162**, 357.
Cane, H. V., Erickson, W. C.: 2005, *Astrophys. J.* **623**, 1180.
Chen, P. F., Fang, C., Shibata, K.: 2005, *Astrophys. J.* **622**, 1202.
Chertok, I. M., Grechnev, V. V.: 2005, *Solar Phys.* **229**, 95.
Chertok, I. M., Grechnev, V. V., Uralov, A. M.: 2009, *Astron. Rep.* **53**, 355.
Cliver, E. W., Nitta, N. V., Thompson, B. J., Zhang, J.: 2004, *Solar Phys.* **225**, 105.
Delaboudinière, J.-P., Artzner, G. E., Brunaud, J. *et al.*: 1995, *Solar Phys.* **162**, 291.
Delannée, C., Aulanier, G.: 1999, *Solar Phys.* **190**, 107.
Gallagher, P. T., Lawrence, G. R., Dennis, B.R.: 2003, *Astrophys. J.* **588**, L53.
Gallagher, P. T., Long, D. M.: 2010, *ArXiv e-prints*, arXiv:1006.0140.
Gopalswamy, N., Yashiro, S., Temmer, M., Davila, J., Thompson, W. T., Jones, S., McAteer, R. T. J., Wuelser, J.-P., Freeland, S., Howard, R. A.: 2009, *Astrophys. J.* **691**, L123.
Grechnev, V. V., Afanasyev, An. N., Uralov, A. M., Chertok, I. M., Eselevich, M. V., Eselevich, V. G., Rudenko, G. V., Kubo, Y.: 2010, *Solar Phys.* Submitted.
Grechnev, V. V., Uralov, A. M., Slemzin, V. A., Chertok, I. M., Kuzmenko, I. V., Shibasaki, K.: 2008, *Solar Phys.* **253**, 263.
Grechnev, V. V., Uralov, A. M., Zandanov, V. G., Rudenko, G. V., Borovik, V. N., Grigorieva, I. Y., Slemzin, V. A., Bogachev, S. A. *et al.*: 2006a, *Pub. Astron. Soc. Japan* **58**, 55.
Grechnev, V. V., Kuzin, S. V., Urnov, A. M., Zhitnik, I. A., Uralov, A. M., Bogachev, S. A., Livshits, M. A., Bugaenko, O. I. *et al.*: 2006b, *Sol. Sys. Res.* **40**, 286.
Grechnev, V. V., Uralov, A. M., Zandanov, V. G.; Baranov, N. Y.; Shibasaki, K.: 2006c, *Pub. Astron. Soc. Japan* **58**, 69.
Handy, B. N., Acton, L. W., Kankelborg, C. C., Wolfson, C. J., Akin, D. J., Bruner, M. E., Caravalho, R., Catura, R. C., *et al.*: 1999, *Solar Phys.* **187**, 229.
Howard, R. A., Moses, J. D., Vourlidas, A., Newmark, J. S., Socker, D. G., Plunkett, S. P., Korendyke, C. M., Cook, J. W. *et al.*: 2008, *Space Sci. Rev.* **136**, 67.
Hudson, H. S., Khan, J. I., Lemen, J. R., Nitta, N. V., Uchida, Y.: 2003, *Solar Phys.* **212**, 121.
Hudson, H. S., Warmuth, A.: 2004, *Astrophys. J.* **614**, L85.
Ichimoto, K., Sakurai, T., Flare Telescope, Norikura Teams: 1993, Proc. 2nd Japan-China seminar on Sol. Phys., p. 151.
Kaiser, M. L., Kucera, T. A., Davila, J. M., St. Cyr, O. C., Guhathakurta, M., Christian, E.: 2008, *Space Sci. Rev.* **136**, 5.
Khan, J. I., Aurass, H.: 2002, *Astron. Astrophys.* **383**, 1018.

Klassen, A., Aurass, H., Mann, G., Thompson, B. J.: 2000, *Astron. Astrophys. Suppl.* **141**, 357.
Landau, L. D., Lifshitz, E. M.: 1987, *Fluid Mechanics*, 2nd edn., Oxford, Pergamon Press.
Long, D. M., Gallagher, P. T., McAteer, R. T. J.. Bloomfield, D. S.: 2008, *Astrophys. J.* **680**, L81.
Low, B. C.: 1982, *Astrophys. J.* **254**, 796.
Low, B. C.: 1984, *Astrophys. J.* **281**, 381.
Magdalenić, J., Marqué, C., Zhukov, A. N., Vršnak, B., Žic, T.: 2010, *Astrophys. J.* **718**, 266.
Magdalenić, J., Vršnak, B., Pohjolainen, S., Temmer, M., Aurass, H., Lehtinen, N.J.: 2008, *Solar Phys.* **253**, 305.
Mancuso, S., Abbo, L.: 2004, *Astron. Astrophys.* **415**, L17.
Mann, G., Klassen, A., Aurass, H., Classen, H.-T.: 2003, *Astron. Astrophys.* **400**, 329.
Meshalkina, N. S., Uralov, A. M., Grechnev, V. V., Altyntsev, A. T., Kashapova, L. K.: 2009, *Pub. Astron. Soc. Japan* **61**, 791.
Moreton, G. E.: 1960, *Astronom. J.* **65**, 494.
Newkirk, G. Jr.: 1961, *Astrophys. J.* **133**, 983.
Pohjolainen, S., Hori, K., Sakurai, T.: 2008, *Solar Phys.* **253**, 291.
Pomoell, J., Vainio, R., Kissmann, R.: 2008, *Solar Phys.* **253**, 249.
Reiner, M. J., Vourlidas, A., Cyr, O.C.S., Burkepile, J. T., Howard, R. A., Kaiser, M. L., Prestage, N. P., Bougeret, J.-L.: 2003, *Astrophys. J.* **590**, 533.
Rudenko, G. V., Grechnev, V. V.: 1999, *Astronomical Data Analysis Software and Systems VIII*, ASP Conf. Series, **172**, 421.
Rudenko, G. V.: 2001, *Solar Phys.* **198**, 5.
Saito, K.: 1970, *Ann. Tokyo Astr. Obs.* **12**, 53.
Schmidt, J. M., Ofman, L.: 2010, *Astrophys. J.* **713**, 1008.
Sheeley, N. R., Jr., Hakala, W. N., Wang, Y.-M.: 2000, *J. Geophys. Res.* **105**, A3, 5081.
Temmer, M., Veronig, A. M., Vršnak, Rybák, J., Gömöry, J., Stoiser, S., Maričić, D.: 2008, *Astrophys. J.* **673**, L95.
Thompson, B. J., Gurman, J. B., Neupert, W. M., Newmark, J. S., Delaboudinière, J.-P., St. Cyr, O. C., Stezelberger, S., Dere, K. P.: 1999, *Astrophys. J.* **517**, L151.
Thompson, B. J., Plunkett, S. P., Gurman, J. B., Newmark, J. S., St. Cyr, O. C., Michels, D. J.: 1998, *Geophys. Res. Lett.* **25**, 2465.
Thompson, B. J., Reynolds, B., Aurass, H., *et al.*: 2000, *Solar Phys.* **193**, 161.
Uchida, Y.: 1968, *Solar Phys.* **4**, 30.
Uchida, Y.: 1974, *Solar Phys.* **39**, 431.
Uralov, A. M., Grechnev, V. V., Hudson, H. S.: 2005, *J. Geophys. Res.* **110**, A05104.
Uralova, S. V., Uralov, A. M.: 1994, *Solar Phys.* **152**, 457.
Veronig, A. M., Muhr, N., Kienreich, I. W., Temmer, M., Vršnak, B.: 2010, *Astrophys. J.* **716**, L57.
Veronig, A. M., Temmer, M., Vršnak, B.: 2008, *Astrophys. J.* **681**, L113.
Vourlidas, A., Wu, S. T., Wang, A. H., Subramanian, P., Howard, R. A.: 2003, *Astrophys. J.* **598**, 1392.
Vršnak, B., Cliver, E. W.: 2008, *Solar Phys.* **253**, 215.
Wang, Y., Zhang, J., Shen, C.: 2009, *J. Geophys. Res.* **114**, 10104.
Warmuth, A., Vršnak, B., Aurass, H., Hanslmeier, A.: 2001, *Astrophys. J.* **560**, L105.
Warmuth, A., Vršnak, B., Magdalenić, J., Hanslmeier, A., Otruba, W.: 2004a, *Astron. Astrophys.* **418**, 1101.
Warmuth, A., Vršnak, B., Magdalenić, J., Hanslmeier, A., Otruba, W.: 2004b, *Astron. Astrophys.* **418**, 1117.
Wills-Davey, M. J., Attrill, G. D. R.: 2009, *Space Sci. Rev.* **149**, 325.
White, S. M., Thompson, B. J.: 2005, *Astrophys. J.* **620**, L63.
Yang, H. Q., Chen, P. F. 2010, *Solar Phys.* **266**, 59.
Yashiro, S., Gopalswamy, N., Michalek, G., St. Cyr, O. C., Plunkett, S. P., Rich, N. B., Howard, R. A.: 2004, *J. Geophys. Res.* 109, A07105.
Zhukov, A. N., Auchère, F.: 2004, *Astron. Astrophys.* **427**, 705.
Zhukov, A. N., Rodriguez, L., de Patoul, J.: 2009, *Solar Phys.* **259**, 73.